In situ carbonation of peridotite for CO$_2$ storage

Peter B. Kelemen[1] and Jürg Matter

Lamont–Doherty Earth Observatory, Columbia University, Palisades, NY 10964

The rate of natural carbonation of tectonically exposed mantle peridotite during weathering and low-temperature alteration can be enhanced to develop a significant sink for atmospheric CO$_2$. Natural carbonation of peridotite in the Samail ophiolite, an uplifted slice of oceanic crust and upper mantle in the Sultanate of Oman, is surprisingly rapid. Carbonate veins in mantle peridotite in Oman have an average ^{14}C age of $\approx$26,000 years, and are not 30–95 million years old as previously believed. These data and reconnaissance mapping show that $\approx$10^4 to 10^5 tons per year of atmospheric CO$_2$ are converted to solid carbonate minerals via peridotite weathering in Oman. Peridotite carbonation can be accelerated via drilling, hydraulic fracture, input of purified CO$_2$ at elevated pressure, and, in particular, increased temperature at depth. After an initial heating step, CO$_2$ pumped at 25 or 30 °C can be heated by exothermic carbonation reactions that sustain high temperature and rapid reaction rates at depth with little expenditure of energy. In situ carbonation of peridotite could consume >1 billion tons of CO$_2$ per year in Oman alone, affording a low-cost, safe, and permanent method to capture and store atmospheric CO$_2$.

alteration and weathering | carbon capture | exothermic | carbon sequestration | mineral

Recognition that anthropogenic CO$_2$ input to the atmosphere has substantially increased atmospheric CO$_2$ concentration, and that increased CO$_2$ may drive rapid global warming, has focused attention on carbon capture and storage (1). One storage option is conversion of CO$_2$ gas to stable, solid carbonate minerals such as calcite (CaCO$_3$) and magnesite (MgCO$_3$) (2). Natural carbonation of peridotite by weathering and low-temperature alteration is common. Enhanced natural processes in situ may provide an important, hitherto neglected alternative to ex situ mineral carbonation "at the smokestack." In this article, we evaluate the rate of natural carbonation of mantle peridotite in the Samail ophiolite, Sultanate of Oman, and then show that under certain circumstances exothermic peridotite alteration (serpentinization, carbonation) can sustain high temperature and rapid reaction with carbonation up to 1 million times faster than natural rates, potentially consuming billions of tons of atmospheric CO$_2$ per year. In situ mineral carbonation for CO$_2$ storage should be evaluated as an alternative to ex situ methods, because it exploits the chemical potential energy inherent in tectonic exposure of mantle peridotite at the Earth's surface, does not require extensive transport and treatment of solid reactants, and requires less energy for maintaining optimal temperature and pressure.

Tectonically exposed peridotite from the Earth's upper mantle, and its hydrous alteration product serpentinite, have been considered promising reactants for conversion of atmospheric CO$_2$ to solid carbonate (3). However, engineered techniques for ex situ mineral carbonation have many challenges. Kinetics is slow unless olivine and serpentine reactants are ground to powder, heat-treated, and held at elevated pressure and temperature (4).* Pending further improvements, these approaches may be too expensive in financial terms and energy expenditures (5).
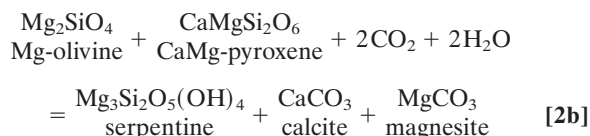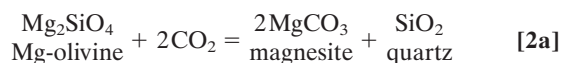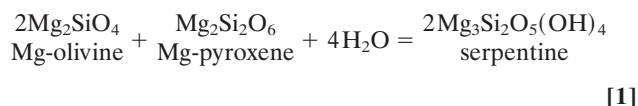
The potential for in situ mineral carbonation in peridotite is emphasized in the following simple calculation. There are $\approx$2.9·10^{15} kg of CO$_2$ in the atmosphere, up from a preindustrial value of perhaps 2.2·10^{15} kg (6). In Oman, the Samail "ophio-lite"—a thrust-bounded slice of oceanic crust and upper mantle—is >350 km long and $\approx$40 km wide, and it has an average thickness of $\approx$5 km (7). Of this volume $\approx$30% is mantle peridotite. Adding 1 wt% CO$_2$ to the peridotite would consume ¼ of all atmospheric CO$_2$, an amount approximately equivalent to the increase since the industrial revolution. Converting all Mg cations in the peridotite to carbonate would consume $\approx$7·10^{16} kg (77 trillion tons) of CO$_2$. Similarly large ophiolites are in Papua New Guinea ($\approx$200 × 50 km in area), New Caledonia ($\approx$150 × 40 km), and along the east coast of the Adriatic Sea (several $\approx$100 × 40 km massifs).

Mantle peridotite is ordinarily beneath the Earth's crust, >6 km below the seafloor and 40 km below the land surface. It is strongly out of equilibrium with air and water at the Earth's surface. Its exposure via large thrust faults along tectonic plate boundaries creates a reservoir of chemical potential energy. Fyfe (8) proposed that exothermic hydration (forming serpentine minerals) can heat peridotite. His idea has recently been invoked to explain the heat source for $\approx$90 °C fluids at the Lost City hydrothermal vent system near the Mid-Atlantic Ridge (9), and evaluated theoretically (10, 11). Below, we show that carbonation of peridotite generates more power than hydration because of larger enthalpy changes and faster reactions between 25 and 200 °C. Temperatures necessary for rapid reaction can be sustained via exothermic carbonation, instead of an external heat source.

Natural Peridotite Hydration and Carbonation

Mantle peridotite is composed largely of the minerals olivine [(Mg,Fe)$_2$SiO$_4$] and pyroxene [(Ca,Mg,Fe)$_2$Si$_2$O$_6$], which react with H$_2$O and CO$_2$ near the Earth's surface to form hydrous silicates (serpentine), Fe-oxides (magnetite), and carbonates (calcite, magnesite, and dolomite). Such reactions may generally be formulated as:

$$\underset{\text{Mg-olivine}}{2Mg_2SiO_4} + \underset{\text{Mg-pyroxene}}{Mg_2Si_2O_6} + 4H_2O = \underset{\text{serpentine}}{2Mg_3Si_2O_5(OH)_4}$$

[1]

$$\underset{\text{Mg-olivine}}{Mg_2SiO_4} + 2CO_2 = \underset{\text{magnesite}}{2MgCO_3} + \underset{\text{quartz}}{SiO_2}$$

[2a]

$$\underset{\text{Mg-olivine}}{Mg_2SiO_4} + \underset{\text{CaMg-pyroxene}}{CaMgSi_2O_6} + 2CO_2 + 2H_2O$$

$$= \underset{\text{serpentine}}{Mg_3Si_2O_5(OH)_4} + \underset{\text{calcite}}{CaCO_3} + \underset{\text{magnesite}}{MgCO_3}$$
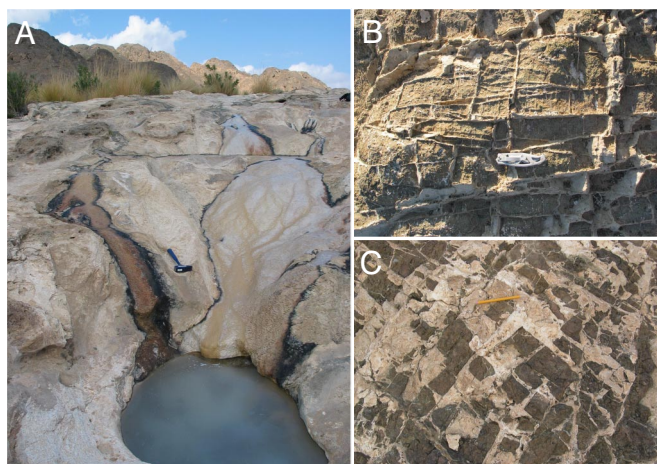
[2b]

GEOLOGY

Fig. 1. Photographs of travertine and carbonate veins in Oman. (*A*) Actively depositing travertine near the village of Falaij (22.846°N, 58.056°E) with rock hammer for scale, altered peridotite in the background. (*B*) White carbonate veins weathering out in positive relief in altered peridotite at ''Duck'' (22.815°N, 58.838°E) with pocket knife for scale. (*C*) White carbonate veins in altered peridotite north of the village of Batin (22.925°N, 58.671°E) with pencil for scale.

Evidence for natural, low-temperature hydration and carbonation of mantle peridotite can be found in springs and associated travertines in catchments composed of mantle peridotite (12–19), and in outcrops of altered peridotite with abundant carbonate veins (e.g., refs. 20–26). High alkalinity, stable isotope ratios, and formation of travertine and carbonate cemented conglomerates in springs (Fig. 1*A*) indicate ongoing serpentinization involving meteoric water at low temperature. In addition to travertine at springs, carbonate veins are also found within host peridotite (Fig. 1 *B* and *C*).

Vein and travertine formation are linked (e.g., refs. 15–19). Groundwater reacting with peridotite in near-surface, open systems forms water rich in Mg and HCO_3^-, which we call *Type 1* waters, according to Barnes and O'Neil (18). When these waters become isolated from the atmosphere, continued reaction with peridotite leads to precipitation of abundant magnesite and dolomite as veins; the resulting waters become progressively richer in Ca and OH^-, and impoverished in dissolved carbon, approaching a pH of 12. When these Ca-OH^--rich, carbon-poor, *Type 2* waters emerge near the surface, to mix with Mg-HCO_3^- waters or react with the atmosphere, they precipitate abundant calcite and dolomite in near-surface veins, carbonate cement in unconsolidated sediment, and travertine.

Rate of Peridotite Carbonation in the Samail Ophiolite, Oman

The rate of CO_2 uptake via weathering of peridotite is poorly known. We sampled solid carbonate forming from peridotite over a wide area in the Samail ophiolite [Fig. 2 and supporting information (SI) Table S1], including veins from ridges far from present day springs as well as currently forming travertine. Previous workers inferred that most veins far from present-day springs are 30–90 million years old, related to formation of oceanic crust, emplacement of the ophiolite, and Eocene extension (e.g., refs. 15, 21, 22, 27). However, all of our samples have ^{14}C ages from 1,600 to 43,000 years, similar to the previously measured range of 840 to 36,000 years in the vicinity of a single, actively forming travertine in Oman (28). Samples of veins from ridges are mainly composed of dolomite and magnesite. In general, they are somewhat older than calcite-rich travertine and calcite-dolomite veins near active springs. However, the vein
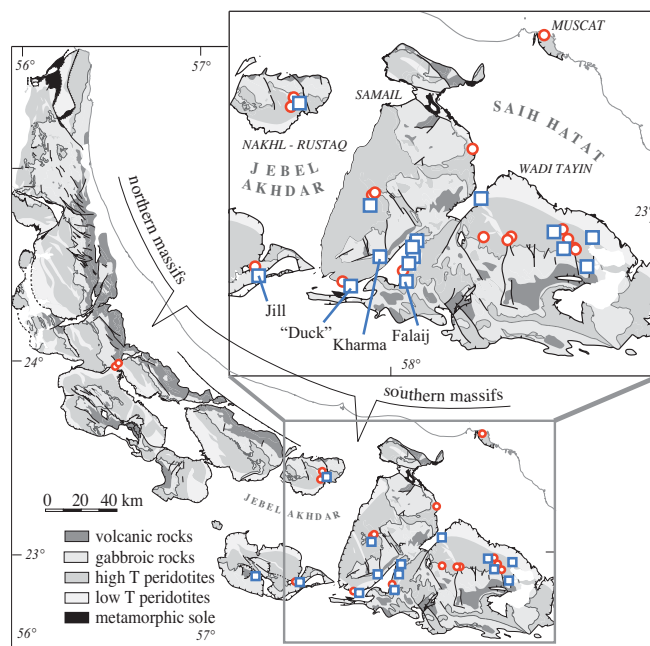

Fig. 2. Geologic map of the Oman ophiolite (8), with locations of carbonate samples dated by using ^{14}C (red circles, Table S1) and locations of known travertine deposits in the Bahla, Samail, and Wadi Tayin ophiolite massifs [blue squares; for perimeter maps of the ''Duck,'' Kharma and Falaij travertines, see Fig. S1; for more information on the Jill travertine deposit, see Clark and Fontes (28)]. Based on our observations of these 3 southernmost massifs, we infer that there are at least 45 similar travertine deposits in the entire ophiolite. We only show locations of travertine deposits that we have personally observed, and there are probably many more even in the southern massifs. In addition to travertine deposits on the surface (Fig. 1*A*, with locations shown here), there are thick travertine deposits forming within alluvial and gravel terraces (examples in Fig. 4).

samples have an average age of ≈26,000 years, with a fairly ''flat'' age distribution (Fig. 3), and none are too old to date with ^{14}C.

The observed volume of carbonate terraces and veins in the Samail ophiolite, together with their ages, can be used to estimate the rate of CO_2 uptake via formation of solid carbonate
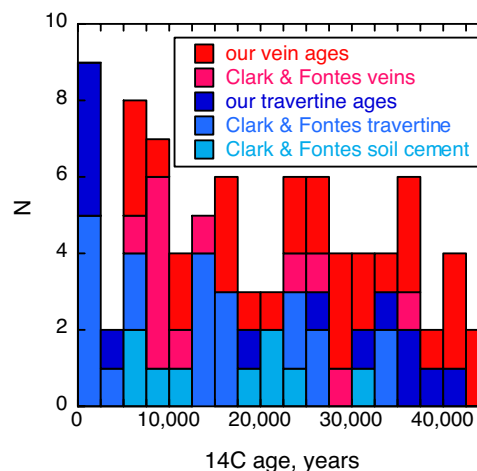

Fig. 3. Combined histogram of ^{14}C ages for our samples (Fig. 2, Table S1) and those of Clark and Fontes (28). The Clark and Fontes samples were taken from a single actively forming travertine deposit near the village of Jill, and carbonate veins in the underlying peridotite within a few meters of the travertine.
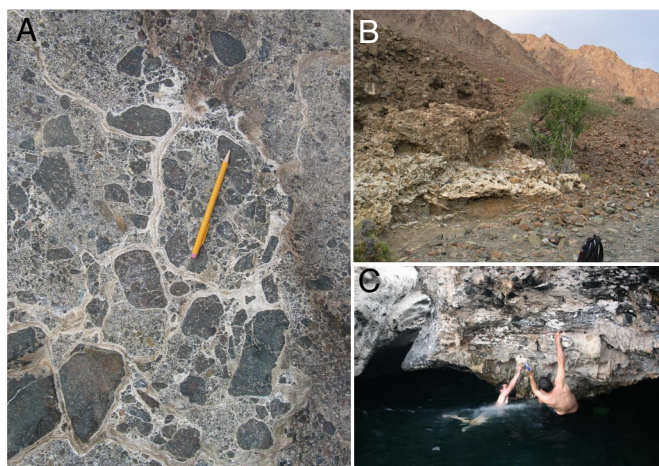
Fig. 4. Carbonate veins and massive travertine ''inflating'' carbonate-cemented, peridotite cobble conglomerate (*A*; 22.9845°N, 58.6322°E) and young alluvial fan deposits (*B*; 22.902°N, 58.371°E). Sampling stalactites forming beneath overhang in peridotite cobble conglomerate (*C*; 22.9875°N, 22.6327°E).

minerals in 2 ways. First, we can estimate the mass of veins directly, and divide this by their average age. Poupeau *et al.* (29) estimated an erosional denudation rate of ≈0.3 mm/yr for northern Oman. The ages of carbonate veins in peridotite suggest that veins form mainly in a thin weathering horizon that keeps pace with erosion; this horizon must generally be ≈15 m thick (erosion rate ≈0.0003 m/yr · maximum age of carbonate veins ≈50,000 years). Newly created road cuts in Oman peridotites reveal abundant, submillimeter carbonate veins on joint surfaces. We measured the vein abundance as ≈1 vol% in transects along road cuts (Table S2); 1% of the volume of a 15-m-thick weathering horizon in the Oman peridotite corresponds to ≈10^{12} kg of CO_2, for an average CO_2 uptake of ≈$4 \cdot 10^7$ kg/yr.

We can independently estimate the mass of travertine formed at and near the surface by alkaline springs, and infer the associated mass of carbonate veins far from the surface that must be formed during recharge of these springs. Based on our relatively detailed, although incomplete, mapping in the southern third of the ophiolite, we estimate that there are ≈45 travertine terraces in the Samail ophiolite (Fig. 2) that are ≈1 m thick, with exposed areas ≈200,000 m^2 (Fig. S1), comprising a total of ≈10^7 m^3 of exposed travertine. Travertine extends beneath alluvium downslope from outcrop areas, and travertine deposits are underlain by a zone ≈10 m thick with ≈5% calcite-rich veins (Table S2), so that their total volume is probably ≈2.5 times the exposed volume. Near-surface deposits, similar in composition and age to the travertine terraces, occur as massive carbonate bands, veins, and cement in alluvial terraces and conglomerates with peridotite clasts (Fig. 4). The volume of carbonate cement derived from Ca-OH$^-$ waters in peridotite sediments is hard to estimate, but is at least as large as the volume of travertine terraces. All of these factors, taken together, suggest that the volume of near-surface travertine and carbonate in peridotite sediments in Oman is ≈$5.5 \cdot 10^7$ m^3 or more, corresponding to at least ≈10^{11} kg of CO_2.

Spring waters and shallow groundwater in peridotite catchments fall into 2 compositional groups, as discussed above and illustrated in Fig. S2. We can estimate carbonation rates from water compositions, assuming (*i*) all carbon in type 1 waters is consumed to form solid carbonate during formation of type 2 waters, and (*ii*) the difference in Ca between type 2 and type 1 waters is precipitated as calcite when type 2 waters reach the

surface. In California, type 1 waters have ≈0.2 mmol of Ca per liter, and up to 24 mmol of carbon per liter (19). Type 2 waters have essentially no carbon, and ≈1.5 mmol Ca per liter (Fig. S2). Thus, for every mole of calcite near the surface, up to ≈24/(1.5–0.2) or 18 mol of magnesite form in the subsurface.

There is a maximum of ≈8 mmol/L, carbon in Oman Type 1 waters, lower than in California, whereas Ca concentration is ≈0.8 mmol/L, higher than in California. There is essentially no carbon, and ≈1.6 mmol Ca in type 2 waters in Oman. It is not clear whether these values reflect lower carbon concentrations in Oman waters compared with those in California, or whether end-member type 1 waters in Oman have not yet been sampled. If, for every mole of near-surface calcite, 8/(1.6–0.8) or 10 mol of magnesite are precipitated as veins, this yields ≈10^{12} kg of CO_2 in veins, consistent with the estimate derived from measured vein abundance and the inferred thickness of the veined horizon.

In summary, estimates of the volume of carbonate deposits formed during ongoing weathering of peridotite, and their average age of 26,000 years, indicate that ≈$4 \cdot 10^7$ kg of atmospheric CO_2 per year are consumed via mineral carbonation in the Samail ophiolite, or ≈2 tons/km^3 of peridotite. This strikingly rapid rate is compared with CO_2 flux in rainwater and groundwater, and discussed further in the *SI Text*. Here, we emphasize that a factor of 100,000 increase in this rate could consume 4 billion tons of CO_2 per year, ≈10% of the annual increase in atmospheric CO_2 because of anthropogenic emissions, via carbonation of peridotite in Oman.

Enhancing Rates of Peridotite Carbonation in Situ

In this section, we propose and evaluate ways to increase CO_2 uptake in situ in tectonically exposed peridotite massifs. In the Samail ophiolite and other large massifs, an obvious approach is to increase the depth of the weathering horizon by a factor of 200, from ≈15 m to ≈3 km in the peridotite via drilling and hydraulic fracture (30). Additional fracture may be anticipated as a result of thermal expansion during heating (31), volume increase during hydration (32–34), and volume increase during carbonation. Carbonation of olivine (Eq. **2b**) results in ≈44% increase in the solid volume, which can lead to enormous stresses that may be relieved by cracking and additional expansion (Fig. 1 *B* and *C*).

An additional increase in the carbonation rate, by a factor of > ≈10^6, could be achieved by raising the temperature of the peridotite and injecting CO_2-rich fluids. There is an optimal temperature for peridotite carbonation. Heating from low temperature speeds the diffusive kinetics of hydration and carbonation. However, the chemical potential driving the reaction is reduced as the temperature approaches the equilibrium phase boundary for serpentine or carbonate mineral stability. The combined effect yields a maximum reaction rate at a temperature intermediate between surface conditions and the equilibrium phase boundary (Fig. S3). The reaction rate for serpentinization as a function of temperature has a maximum value at ≈260 °C over a range of pressure (35), whereas the rate of carbonation is optimized at, for example, 185 °C and 150 bars CO_2 pressure.* We fit data on rates of serpentinization of olivine with grain size 58–79 μm (35) and carbonation of olivine with grain size ≤75 μm* as a function of temperature and CO_2 partial pressure, yielding a serpentinization rate (Fig. S4)

$$\Gamma = 0.00000100 \exp[-0.000209(T - 260°C)^2] \quad [3]$$

and a carbonation rate (Fig. S5 and Fig. S6).

$$\Gamma \sim 1.15 \cdot 10^{-5}(P(CO_2), bars)^{1/2} \exp[-0.000334(T - 185°C)^2] \quad [4]$$
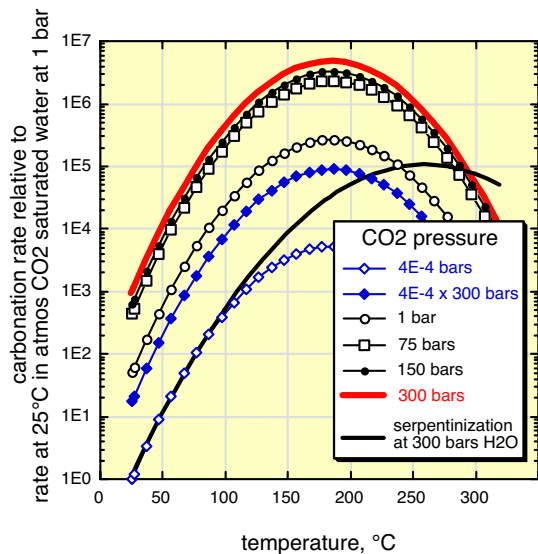
GEOLOGY

Fig. 5. Rates of olivine carbonation (lines and symbols) and serpentinization (black line, no symbols) as a function of temperature and pressure, compared with the rates at 25 °C for surface water equilibrated with the atmosphere at 1 bar. A range of curves are shown for carbonation, with a single curve for serpentinization of olivine saturated in aqueous fluid at 300 bars. Note that the reaction rate for carbonation is much higher than that for serpentinization at 300 bars and temperature < ≈250 °C. The enthalpy change, per kilogram, is also ≈3 times larger for carbonation than for serpentinization (see text).

both in units of mass fraction per second. Heating and raising the partial pressure of CO_2 can increase the carbonation rate by a factor of >10^6 (Fig. 5), and with the potential for increasing the

thickness of the weathering horizon by fracturing, the overall increase could be a factor of ≈10^9. Together with the estimated present-day CO_2 uptake at the end of the previous section, this corresponds to 2·10^9 tons/km³ per year.

Thermal Effects of Advection, Diffusion, and Reaction

The change in temperature for a particular volume in a subsurface, porous aquifer can be approximated in 1 dimension as

$$dT/dt = (T_{in} - T)\rho_f C_p^f \phi w/(\rho_s C_p^s d) - (T - T_o)\kappa/d^2$$
$$+ \Gamma(T)A\Delta H/[C_p^s(1 - \phi) + C_p^f(\phi)] \quad \textbf{[5]}$$

where T_{in} is the temperature of incoming water or aqueous fluid (°C or Kelvin), T is the current temperature in the volume, T_o is the far-field temperature, outside the volume, which is equal to the initial temperature in the volume, ρ_f and ρ_s are the densities of the fluid and solid, C_p^f and C_p^s are the heat capacities of the fluid and solid, ϕ is the porosity or volume fraction of fluid (nondimensional, 1% in all calculations shown here), w is the fluid flow velocity (m/s), d is the dimension or "size" of the volume (m, 1,000 m in all calculations shown here), κ is the thermal diffusivity (10^{-6} m²/s), Γ is the reaction rate, which is a function of temperature (units of 1/s), A is the fraction of the rock available for reaction in the volume (nondimensional), and ΔH is the enthalpy change due to reaction. The use of a reactive volume fraction term <1 accounts for the fact that most natural rocks do not have an effective grain size of ≈70 μm, unlike the experiments used to calibrate Eqs. **3** and **4**. The volume available for reaction is product of a diffusion distance times the surface area of grains. The surface area is proportional to the radius squared, so the use of a reactive volume fraction of 0.01% corresponds to modeling of an effective "grain size" or fracture spacing of ≈7 mm, 100 times larger than in the experiments.
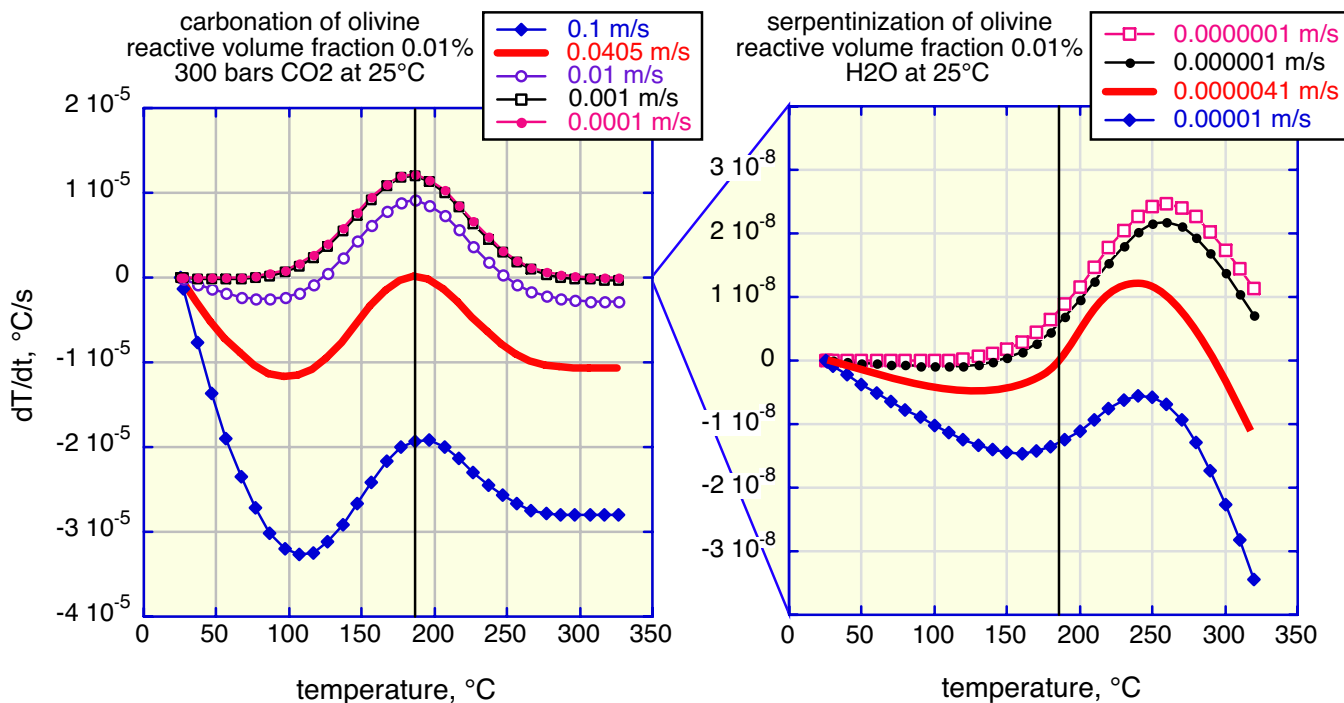

Fig. 6. Calculated rate of change of temperature due to olivine carbonation (*Left*) and serpentinization (*Right*) at 300 bars as a function of rock temperature and fluid flow rate, for 25 °C fluid and a reactive volume fraction of 0.01%, from our 1-dimensional energy balance model (Eq. **5**). A constant rock temperature of 185 °C can be maintained by pumping 25 °C CO_2 at ≈0.040 m/s, or by pumping 25 °C H_2O at ≈4.1·10^{-6} m/s. Note that the range of temperature derivatives and steady-state flow rates at 185 °C are much larger for the olivine carbonation reaction than for serpentinization.
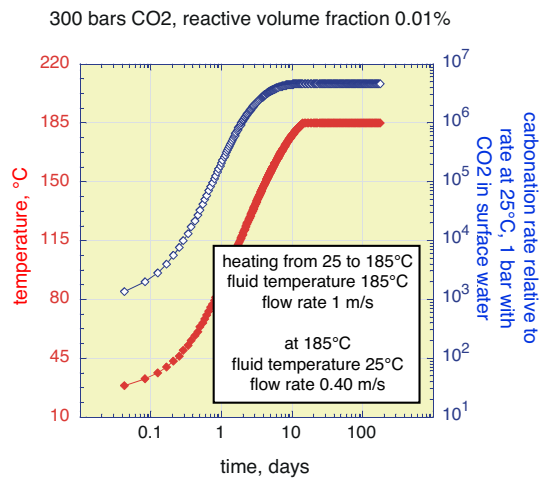
300 bars CO2, reactive volume fraction 0.01%

Fig. 7. Calculated temperature and carbonation rate, relative to the rate at 25 °C for CO_2 in surface water at equilibrated with the atmosphere at 1 bar, for a 3-step method beginning with drilling and hydraulic fracture, followed by heating via rapid pumping of 185 °C CO_2, followed by slower pumping of 25 °C CO_2 to maintain constant temperature.

For these calculations, densities, heat capacities, and enthalpies were obtained from standard references reviewed and updated by Gottschalk (36) and similar data from the National Institute of Standards (NIST) Chemistry WebBook (NIST Standard Reference Database Number 69, June 2005 Release) at http://webbook.nist.gov/chemistry/. For our calculations, we fit simple functions to the temperature dependence of thermodynamic properties from 25 to 300 °C. For H_2O and CO_2, we used 300 bars pressure for the calculations discussed in this section. Above 300 °C, and far from this pressure, our calculations would be inaccurate.

Fig. 6 illustrates results from Eq. **5** in terms of temperature change, dT/dt, versus initial temperature, for fluid porosity of 0.01 (1%), fluid temperature of 25 °C at 300 bars pressure, with reactive volume fraction A of 0.01%. At high flow rates with cold (25 °C) fluid, the volume cannot be heated by exothermic reactions. At low flow rates, advective cooling is negligible, and temperature is controlled by exothermic heating and diffusive cooling. To optimize olivine carbonation rates, fluid flow should be adjusted to yield $dT/dt = 0$ at ≈185 °C. Heating due to hydration (serpentinization) is less effective than heating due to carbonation. This is partly because, for example, at 1 bar and 25 °C, ΔH is ≈250 kJ/kg for serpentinization (Eq. **1**), whereas carbonation (Eq. **2**) evolves ≈760 kJ/kg, and partly because serpentinization is slower than carbonation for temperatures between 25 and 185 °C (Fig. 5).

Recipes for in Situ Carbonation of Peridotite

One approach is to take maximum advantage of the exothermic heat output available from the carbonation reaction, by raising a rock volume to the optimal temperature for peridotite carbonation. To reach and maintain 185 °C, it is necessary to preheat the rock volume. This can be achieved via a variety of flow rates, fluid temperatures, and fluid compositions. Initial heating should probably be via high flow rates by using preheated fluids. Later, because large volumes of rock are to be held at 185 °C to optimize CO_2 uptake, output fluid can be used to heat other areas. This may happen spontaneously as hot fluid flows into colder, surrounding rock.

Because pumping rates for 25 °C fluid must remain low to maintain high temperature, dissolved CO_2 in surface water cannot be supplied rapidly enough to keep pace with the enhanced carbonation rates modeled here. Instead, injection of
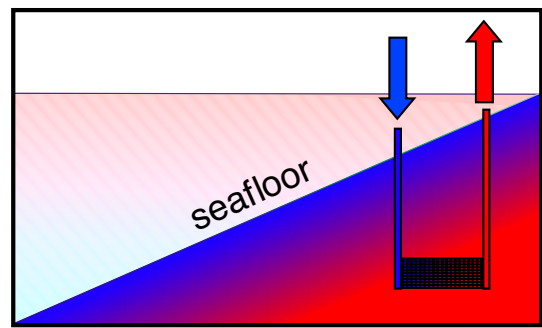

Fig. 8. Schematic representation of 2 bore holes into peridotite below the seafloor, connected by a fracture network. Color gradients below the seafloor represent temperature variation with blue indicative of ≈0–25 °C and red indicative of ≈150 °C. As a result of thermal convection, near-surface seawater would descend one hole (with a controlled flux) and rise through the other. At depth, the water would be heated by the geothermal gradient and by exothermic serpentinization and carbonation reactions. Mineral carbonation in the peridotite would consume dissolved CO_2 from evolving seawater along the flow path.

pure CO_2, or a CO_2-rich fluid mixture, is required to keep pace with the enhanced reaction rate. As seen in Fig. 6, dT/dt resulting from carbonation is zero at 185 °C when the flow rate of pure CO_2 injected at 300 bars and 25 °C is ≈0.040 m/s and the reactive volume fraction is 0.01%. At these conditions, our 1-dimensional model delivers ≈0.166 kg of CO_2 per s to a $1 \times 1 \times 1000$ m³ rock volume, and consumes ≈0.127 kg of CO_2 per s to form solid magnesite. All olivine is consumed after ≈190 days, consuming ≈2,000 tons of CO_2 per 1,000 m³, or—scaling up—2·10⁹ tons of CO_2 per km³ at ≈4·10⁹ tons/yr. Note that this is an *independent estimate* of CO_2 uptake, which is consistent with the rate of ≈2·10⁹ tons/km³ per year derived at the end of the section entitled *Enhancing Rates of Peridotite Carbonation in Situ*.

Fig. 7 provides an example of a 3-step process, with drilling and hydrofracture of peridotite at depth, followed by injection of hot fluid to heat the newly fractured peridotite to 185 °C, followed in turn by injection of pure CO_2 at 25 °C to sequester carbon whereas exothermic carbonation maintains the system at 185 °C. Our simple calculations show that a factor of more than 1 million enhancement in the carbonation rate is achievable. Note that we have not incorporated the "cost-free" heating afforded by the geothermal gradient; if northern Oman lies along a typical continental geotherm of 10–20 °C/km (37), then the initial temperature at the bottom of a 3-km drill hole will be 55–85 °C, not the initial 25 °C used in our model. Indeed, Neal and Stanger (15) report that alkaline springs in Oman peridotites have temperatures up to 15 °C hotter than normal groundwater in the same locations, and infer that the alkaline waters have been heated during circulation at depths of 700 m or more.

Our calculations are done assuming that the reactive volume fraction is constant, whereas, in practice, reactive surfaces may become depleted. It may be necessary to reduce the fluid flow rate as this occurs, to avoid cooling the reacting volume. At some point, in particular, if reaction-driven cracking does not occur, it may be necessary to hydraulically fracture the system again to expose additional reactive surface area. More optimistically, temperature change and the large increases in solid volume due to mineral hydration and carbonation will cause cracking and increased permeability. In any case, eventually all accessible olivine in a given rock volume will be depleted. Before this occurs, fluid heated by reaction in 1 region can be pumped into an adjacent area to begin the process anew.

An alternative process could avoid prolonged pumping of fluid and use of purified CO_2. In Oman, New Caledonia, and Papua New Guinea, peridotite is present beneath a thin veneer

GEOLOGY

of sediment offshore. Here, peridotite could be drilled and fractured, and a volume could be heated. Again, little heating would be required if, for example, the initial temperature at the bottom of a 5-km bore hole is 100 °C (Fig. 8). Then, controlled convection of near-surface water through the rock volume could sustain high temperature via exothermic hydration of olivine at a flow rate of $\approx 4 \cdot 10^{-6}$ m/s (as seen in Fig. 3 *Right*). The carbonation rate would be limited by supply of dissolved CO_2 in convecting seawater—only $\approx 10^4$ tons of CO_2 per km^3 of peridotite per year at a flow rate of $4 \cdot 10^{-6}$ m/s—but the cost would be relatively low.

Conclusion: Promising Alternatives to ex Situ Mineral Carbonation

Because these proposed methods of in situ mineral carbonation use the chemical potential energy inherent in tectonic exposure of mantle peridotite at the Earth's surface, the optimal temperature for carbonation can be maintained in a rock volume at little expense. Further, rock volumes at depth are, inherently, at relatively high pressure and elevated temperature. Thus, compared with engineered, mineral carbonation "at the smokestack," this method does not involve quarrying and transportation of peridotite, processing of solid reactants via grinding and heat treatment, or maintaining high temperature and pressure in a reaction vessel. Instead, the major energy investments in this method would be for drilling, hydraulic fracturing, pumping fluid, preheating fluid for the first heating step, and purification of CO_2. Also, unlike ex situ mineral carbonation, this method may require on-site CO_2 capture or transport of purified CO_2 to the in situ carbonation locality.

Clearly, more elaborate models combined with field tests will be required to evaluate and optimize this method. For example, it is difficult to predict the consequences of hydraulic fracturing of peridotite, plus cracking associated with heating, hydration, and carbonation, in terms of permeability and reactive volume fraction. Such processes are all-but-impossible to simulate in the laboratory. Large-scale field tests should be conducted, because the proposed method of enhanced natural CO_2 sequestration provides a promising potential alternative to storage of supercritical CO_2 fluid in underground pore space, and to engineered, ex situ mineral carbonation.

1. Metz B, Davidson O, de Coninck H, Loos M, Meyer L, eds (2005) *IPCC Special Report on Carbon Dioxide Capture and Storage* (Cambridge Univ Press, New York), p 431.
2. Seifritz W (1990) CO2 disposal by means of silicates. *Nature* 345:486.
3. Lackner KS, Wendt CH, Butt DP, Joyce EL, Sharp DH (1995) Carbon dioxide disposal in carbonate minerals. *Energy* 20:1153–1170.
4. Lackner KS, Butt DP, Wendt CH (1997) Progress on binding CO2 in mineral substrates. *Energy Convers Manage* 38:S259–S264.
5. Mazzotti M, *et al.* (2005) Mineral carbonation and industrial uses of CO2. *IPCC Special Report on Carbon Dioxide Capture and Storage*, eds Metz B, Davidson O, de Coninck H, Loos M, Meyer L (Cambridge Univ Press, Cambridge, UK), pp 319–338.
6. Solomon S, *et al.* (2007) Technical summary. *Climate Change 2007: The Physical Science Basis. Contribution of Working Group I to the Fourth Assessment Report of the Intergovernmental Panel on Climate Change*, eds Solomon S, *et al.* (Cambridge Univ Press, Cambridge, UK), pp 20–91.
7. Nicolas A, Boudier E, Ildefonse B, Ball E (2000) Accretion of Oman and United Arab Emirates ophiolite: Discussion of a new structural map. *Marine Geophys Res* 21(3–4):147–179.
8. Fyfe WS (1974) Heats of chemical reactions and submarine heat production. *Geophys J Roy Astr Soc* 37(1):213–215.
9. Kelley DS, *et al.* (2001) An off-axis hydrothermal vent field near the Mid-Atlantic Ridge at 30 degrees N. *Nature* 412(6843):145–149.
10. Emmanuel S, Berkowitz B (2006) Suppression and stimulation of seafloor hydrothermal convection by exothermic mineral hydration. *Earth Planet Sci Lett* 243(3–4):657–668.
11. Allen DE, Seyfried WE (2004) Serpentinization and heat generation: Constraints from Lost City and Rainbow hydrothermal systems. *Geochim Cosmochim Acta* 68(6):1347–1354.
12. Zedef V, Russell MJ, Fallick AE, Hall AJ (2000) Genesis of vein stockwork and sedimentary magnesite and hydromagnesite deposits in the ultramafic terranes of southwestern Turkey: A stable isotope study. *Econ Geol* 95(2):429–445.
13. Wenner DB, Taylor HPJ (1974) D/H and 18O/16O studies of serpentinization of ultramafic rocks. *Geochim Cosmochim Acta* 38:1255–1286.
14. Weyhenmeyer CE (2000) Origin and evolution of groundwater in the alluvial aquifer of the Eastern Batinah Coastal Plain, Sultanate of Oman. PhD thesis (Geologisches Institut, Universität Bern), 202 pp.
15. Neal C, Stanger G (1985) Past and present serpentinization of ultramafic rocks: An example from the Semail ophiolite nappe of northern Oman. *The Chemistry of Weathering*, ed Drewer JI (D. Reidel Publishing Company, Dordrecht, Holland), pp 249–275.
16. Cipolli F, Gambardella B, Marini L, Ottonello G, Zuccolini MV (2004) Geochemistry of high-pH waters from serpentinites of the Gruppo di Voltri (Genova, Italy) and reaction path modeling of CO2 sequestration in serpentinite aquifers. *Appl Geochem* 19(5):787–802.
17. Bruni J, *et al.* (2002) Irreversible water-rock mass transfer accompanying the generation of the neutral, Mg-HCO3 and high-pH, Ca-OH spring waters of the Genova province, Italy. *Appl Geochem* 17(4):455–474.
18. Barnes I, O'Neil JR (1969) Relationship between fluids in some fresh alpine-type ultramafics and possible modern serpentinization, western United States. *GSA Bull* 80(10):1947–1960.
19. Barnes I, LaMarche VC, Himmelberg G (1967) Geochemical evidence of present-day serpentinization. *Science* 156(3776):830–832.
20. Hansen LD, Dipple GM, Gordon TM, Kellett DA (2005) Carbonated serpentinite (listwanite) at Atlin, British Columbia: A geological analogue to carbon dioxide sequestration. *Can Mineral* 43:225–239.
21. Nasir S, *et al.* (2007) Mineralogical and geochemical characterization of listwaenite from the Semail ophiolite, Oman. *Chemie Der Erde* 67:213–228.
22. Wilde A, Simpson L, Hanna S (2002) Preliminary study of Cenozoic alteration and platinum deposition in the Oman ophiolite. *J Virtual Explorer* 6:7–13.
23. Früh-Green G, Weissert H, Bernoulli D (1990) A multiple fluid history recorded in Alpine ophiolites. *J Geol Soc London* 147:959–970.
24. Trommsdorff V, Evans B, Pfeifer HR (1980) Ophicarbonate rocks: Metamorphic reactions and possible origin. *Arch Sci Genève* 33:3610364.
25. Naldrett AJ (1966) Talc-carbonate alteration of some serpentinized ultramafic rocks south of Timmins, Ontario. *J Petrol* 7:489–499.
26. Stanger G (1985) Silicified serpentinite in the Semail nappe of Oman. *Lithos* 18(1):13–22.
27. Python M, Ceuleneer G, Ishida Y, Barrat J-A, Arai S (2007) Oman diopsidites: A new lithology diagnostic of very high temperature circulation in mantle peridotite below oceanic spreading centers. *Earth Planet Sci Lett* 255:289–305.
28. Clark ID, Fontes JC (1990) Paleoclimatic reconstruction in northern Oman based on carbonates from hyperalkaline groundwaters. *Quat Res* 33(3):320–336.
29. Poupeau G, Saddiqi O, Michard A, Goffé B, Oberhänsli R (1998) Late thermal evolution of the Oman Mountains subophiolitic windows: Apatite fission-track thermochronology. *Geology* 26:1139–1142.
30. Valkó P, Economides MJ (1995) *Hydraulic Fracture Mechanics* (Wiley, Chichester), p 298.
31. Fredrich JT, Wong TF (1986) Micromechanics of thermally induced cracking in 3 crustal rocks. *J Geophys Res* 91:2743–2764.
32. Jamtveit B, Malthe-Sorenssen A, Kostenko O (2008) Reaction enhanced permeability during retrogressive metamorphism. *Earth Planet Sci Lett* 267:620–627.
33. Iyer K, Jamtveit B, Mathiesen J, Malthe-Sorenssen A, Feder J (2008) Reaction-assisted hierarchical fracturing during serpentinization. *Earth Planet Sci Lett* 267:503–516.
34. Fletcher RC, Buss HL, Brantley SL (2006) A spheroidal weathering model coupling porewater chemistry to soil thickness during steady-state denudation. *Earth Planet Sci Lett* 244:444–457.
35. Martin B, Fyfe WS (1970) Some experimental and theoretical observations on kinetics of hydration reactions with particular reference to serpentinization. *Chem Geol* 6(3):185–202.
36. Gottschalk M (1997) Internally consistent thermodynamic data for rock-forming minerals in the system SiO2-TiO2-Al2O3-Fe2O3-CaO-MgO-FeO-K2O-Na2O-H2O-CO2. *Eur J Mineral* 9:175–223.
37. Blackwell DD (1971) The thermal structure of the continental crust. *The Structure and Physical Properties of the Earth's Crust,* Geophysical Monograph 14, ed Heacock JG (American Geophysical Union, Washington, DC), pp 169–184.